Modelling of Rain Radar Image Space-Time Dynamics with Cellular Automata

A. Núñez [1], V. Pastoriza [2], P. Mariño [2], F. P. Fontán [1], and U.-C. Fiebig [3],
[1]University of Vigo
Signal Theory and Communications Department, Campus Universitario Lagoas Marcosende, 36310 Vigo, Spain
fito@tsc.uvigo.es, fpfontan@tsc.uvigo.es
[2]University of Vigo
Electronic Technology Department, Campus Universitario Lagoas Marcosende, 36310 Vigo, Spain
vpastoriza@uvigo.es, pmarino@uvigo.es
[3]German Aerospace Center (DLR)
Institute for Communications and Navigation, D-82230 Wessling, Germany
Uwe.Fiebig@dlr.de

***Abstract*-A straightforward linkage between rain cell dynamics in terms of reflectivity Z (dBz) or its equivalent rain rate R (mm/h) and satellite or terrestrial radiolink attenuation can be performed. This work focuses on the presentation of an approach for assessing and characterizing rain cell dynamics based exclusively on the analysis of the radar reflectivity scans recorded in weather radar image, and without an a priori assumption on the structure of rain cells. This research has been addressed by using cellular automata. Rain cell dynamics are simulated by using probabilistic cellular automata rules and tracking vectors which indicate a global advection direction and velocity.**

I. INTRODUCTION

Spatial and temporal rain dynamics is a research topic of great interest in several fields including, e.g.: hydrology, climatology, weather nowcasting/forecasting, telecommunications. In the radio propagation context, as communication systems using frequencies above about 10 GHz are impaired by rain then attenuation due to rain is an important effect which must be considered. For this reason, several rain induced attenuation models have been developed using meteorological data [1]. In particular, the prediction of that attenuation from rainfall intensity has been the subject of a major effort carried out by many researchers. Several methods modeling space-time rain field dynamics, as previous step to predict attenuation, have been developed and tested following different ways, e.g.: assuming regular shapes of rain cells (ellipses, circles, Gaussian or exponential decay functions, …), using fractal methods, etc. Principal sources of data for studying rainfall are represented by rain gauges, sensors on satellite and meteorological ground based radar. Here, data only from ground based radar will be used.

A straightforward linkage between rain cell dynamics in terms of reflectivity Z (dBz) or its equivalent rain rate R (mm/h) and satellite or terrestrial radiolink attenuation can be performed. In this work, extension of [2], we focus on the presentation of an approach for assessing and characterizing rain cell dynamics based exclusively on the analysis of the radar reflectivity scans recorded in weather radar image (WRI), and without an a priori assumption on the structure of rain cells. This research has been addressed by using cellular automata (CA).

CA are dynamical systems in which space and time are both discrete. CA were originally introduced by Von Neumann [3] and Ulam [4] with the purpose of obtaining self-reproduction biological models. Since then, CA have drawn much interest because of their usefulness as a simple discrete model for many dynamical processes [5-7]. CA have been used in a number of fields including physics, chemistry, biology, economics or information systems. However, finding the CA that displays a desired behavior can be a hard task, especially in complex, real world problems.

A CA consists of a D-dimensional array of sites (lattice), each of which can be in one of a finite number of possible states, and which is updated at discrete time steps, according to a local interaction rule (CA rule) identical for all sites. This rule, and therefore the CA, can be deterministic or probabilistic. A probabilistic CA rule is a probabilistic histogram derived from the frequency of occurrence of each input/output pair found. The state of every site at a time step T is determined by the states of a neighborhood of sites surrounding that site at one or more previous time steps.

In CA context, WRIs have been considered as lattices so each pixel is a site and the operands are that pixel, where the local rule is applied to obtain the next pixel state, together with other pixels in its neighborhood. We show here a method that uses a 2-D, 3-state, 25-site neighborhood probabilistic CA to assess rain cell dynamics contained in WRIs. Rain cell dynamics are simulated by using probabilistic CA rules and tracking vectors.

This work has been partially funded by EU's Network of Excellence SatNexII, CICYT, Spanish Ministry of Education and Science, and the Regional Goverment of Galicia (Spain), Xunta de Galicia.

II. METHOD

In this work, for a given WRI sequence, the simulation of a WRI at any time *T* will be made by means of its corresponding probabilistic CA rule and a tracking vector: one different rule and tracking vector for every two consecutive WRIs (a WRI transition). The proposed method, based on [8] which is an extension of [2], consists of 6 major steps. First the assignment of WRI pixels to 3 categories, no rain (NR), light rain (LR) and heavy rain (HR), is made for all WRIs in the sequence. Secondly, small rainy pixel clusters are removed using a morphological operation. After that, the probabilistic CA rule and the tracking vector for each WRI transition are computed. Then, the simulation is performed. Finally, the same morphological operation is applied to improve the simulated results.

Step 1. 3-category pixel assignment

Although rainfall fields are very complex to describe and classify, two main types of rain are relevant: convective and stratiform. The radar reflectivity images are converted in 3-category images based on this classification to separate NR, LR and HR regions.

The WRIs, where reflectivity is expressed in dBz, are converted to 3-category images. Each dBz pixel value is classified as NR, LR or HR: 0, 1 and 2 respectively. Here, we map intensities below 1mm/h to NR category, from 1 to 10 mm/h to LR category, and intensities exceeding 10 mm/h to HR category [9, 10].

The radar rainfall-reflectivity (*R-Z*) conversion is computed based on the *Z-R* power law relationships of the form $Z = a \cdot R^b$, which is probably the most widely used one in the literature for a quick and straightforward conversion of a certain radar reflectivity Z (mm^6/m^3) to radar rain rate R (mm/h). The relationships

$$Z = 200 \cdot R^{1.6} \tag{1}$$

has been used in this study [11]. WRIs were converted to 3-category images by using the Z thresholds of 23 dBz and 39 dBz that correspond to 1 mm/h and 10 mm/h rain rate respectively.

Step 2. Removing of small rainy pixel clusters

After WRI discretization, small rainy pixel clusters are removed by means of a morphological operation in order to simplify the images to be process. Such operation, named area thresholding, consists of 3 stages. First LR and HR pixels are converted to a single rainy category. Then the resulting rainy clusters of area smaller than 5 pixels are removed (converted to NR category). Finally, the pixels of the remaining rainy pixels are restored to their original categories. The area threshold value of 5 has been chosen after a tradeoff study.

Step 3. Computation of probabilistic CA rule

Currently a different probabilistic CA rule for every WRI transition in the sequence is computed. In this paper, we consider that the CA rule for a given transition is the probabilistic table (ptable) of that transition, and where the ptable is the probabilistic histogram derived from the frequency of occurrence of each input/output pair found for that transition.

The ptable for a given *T1-T2* transition, where *T2* is any time and *T1* is the immediately previous time (*T1* = *T2*–10 min), is obtained in two stages. First, the ptable input states are computed from the input states of WRI pixels at time *T1*. Then the matching between pixel input states at time *T1* to pixel category values at time *T2* is based on the highest mutual information criterion.

Stage 3.1. Computing of ptable input states: The input state for each WRI pixel at time *T1 P(x,y,T1)* is determined by a neighborhood of 27×27 pixels surrounding and including *P(x,y,T1)*. This input neighborhood (INH) is arranged in a pyramid structure with three levels of detail (Fig. 1) in such a way that rain cell dynamic effects in the *T1-T2* transition can be captured with it. The INH consists of 25 sites, organised in these 3 pyramid levels, and where the 1st site is *P(x,y,T1)*. Each site of the first level takes a category value of 0, 1 or 2 as a function of its rain type. Then, the category value of a site belonging to the second pyramid level is computed as the first pyramid level site amount of each category that forms that site plus a thresholding algorithm (Table I). Finally, the category value of a third pyramid level site is computed as the second pyramid level site amount of each category that forms that third level site plus that thresholding algorithm.

In that thresholding algorithm, a_j denotes the category value at the j-th site of m-th pyramid level, while a_{ij} indicates the category value of the 9 sites with (m–1)-th pyramid level that make up the j-th site. *K_thres* is a vector of 2 elements (num-

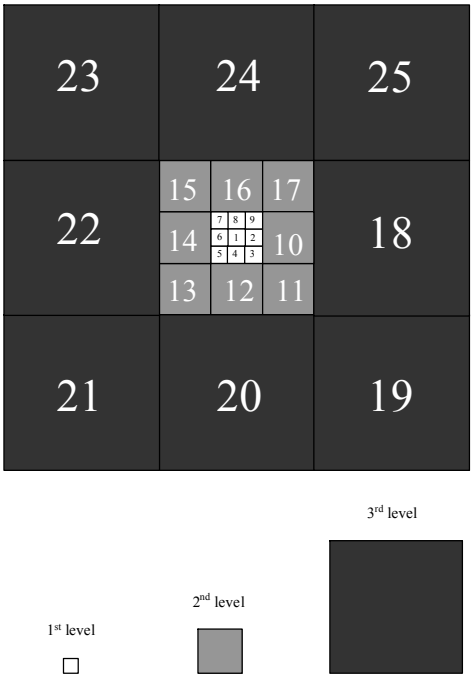

Fig. 1. Pyramid structure with 3 levels.

TABLE I
THRESHOLDING ALGORITHM

$\forall\ j \in \{10, \ldots, 25\}$

$a_j = 0$

$n_1 = Number\_of\_Sites(\ a_{ij} == 1)$

$n_2 = Number\_of\_Sites(\ a_{ij} == 2)$

if $n_1 > K\_thres(1)$ and $n_2 <= K\_thres(2)$ then $a_j = 1$

if $n_2 > K\_thres(2)$ then $a_j = 2$

ber of categories minus one), where each element can be an integer value between 0 and 9 (maximum possible amount of sites). The choice criterion of the *K_thres* vector values for a particular *T1-T2* transition will be explained later on. The input state for each *P(x,y,T1)* is computed as

$$input\ state\ value = \sum_{j=1}^{25} a_j \cdot 3^{j-1} \qquad (2)$$

where $a_j \in \{0, 1, 2\}$.

Finally, the ptable input states are the unique pixel input states at time *T1* computed.

Stage 3.2. Matching: The input state of each WRI pixel at time *T1 P(x,y,T1)* is matched to the category value of the pixel at time *T2* belonging to the 9x9 pixel box centred at *P(x,y,T2)* which yields the ptable with the highest mutual information (Fig. 2).

The *K_thres* vector values chosen in the thresholding algorithm to compute the input states are those which give the ptable with the highest mutual information, the ptable is derived from the frequency of occurrence of each input/output pair, and the mutual information (MI) is a measure of the amount of information that one random variable contains about another random variable [12, 13]. MI is defined by

$$MI(x,y) = \sum_{i,j} P(x_i,y_j) \cdot \log \frac{P(x_i,y_j)}{P(x_i) \cdot P(y_j)} \qquad (3)$$

where $P(x_i)$ is the probability of the state variable x being in the discrete state i, and $P(x_i, y_j)$ is the joint probability. In this case it can be seen as a measure of the correlation between the pixel input state and its corresponding pixel category value.

Step 4. Computing of the tracking vector

In the previous step, it is worth noting that all input/output pairs computed for a ptable have the same displacement relation between their pixel input state and their corresponding pixel category value, i.e., the input state at any *P(x,y,T1)* is matched with the category value at *P(x+dx,y+dy,T2)*. The later being the pixel belonging to the 9x9 pixel box centred at *P(x,y,T2)* which gives the ptable with the highest mutual information (Fig. 2).

This displacement relation is represented by [*dx,dy*], which indicates the average movement vector (tracking vector) of the *T1-T2* transition. In general different *T1-T2* transitions have different tracking vectors.

Step 5. Simulation

The simulation of a WRI at any time *T* will be made by first computing the input state for each pixel of WRI at time *T*–10 min *P(x,y,T–10)*. Then the simulated category value of each pixel of WRI at time *T P(x,y,T)* is worked out from the probabilistic CA rule, and finally the *P(x,y,T)* category value is assigned to *P(x+dx,y+dy,T)* using the corresponding tracking vector.

Step 6. Final improvement

Finally, the same morphological operation as in step 2 is applied to the resulting simulated image to remove isolated small rainy pixel clusters.

III. Results and Analysis

The data source used in this study is the radar reflectivity scan recorded to a WRI every 10 minutes by the weather radar of the Spanish Meteorological Office, which is located at Cerceda, A Coruña, in the North-West of Spain, at latitude 43º 10' 16'' N, longitude -8º 31' 26'' E/W, and height 621 m asl. The results presented in this work are obtained from one

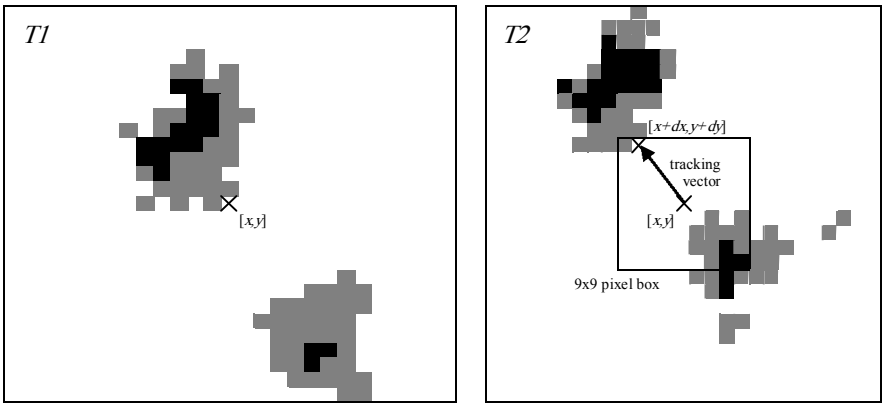

Fig. 2. Schematic showing the tracking vector of the *T1-T2* transition.

hundred different examples containing heavy rain regions and each example consists of 18 WRIs (3 hours). The simulated WRI area consists of a 135x135 pixel area with a spatial resolution of 1x1 km^2 per pixel.

To quantify or rate the performance of the simulations, actual data and simulated results have to be compared. For this purpose the *K*-category correlation coefficient *Rk* [14] which is an extended Matthews's correlation coefficient [15] has been used. Here, the focus is in particular on a three-category problem (types of rain: NR, LR, HR). Due to the intrinsic variability of *Rk* we have performed 100 realizations per example, and the average of the 100 *Rk* computed is taken as the *Rk* of that example. Results are summarized in Table II. *K*-category correlation coefficient values of the best example, the worst one and the averaged value are shown. Table II also reflects the slight increase in *Rk* when a final improvement (morphological operation in the step 6) is applied to remove isolated small rainy pixel clusters.

It is worth noting that the method proposed not only provides simulation capability but it also allows extracting a common motion vector for entire rain cells of WRI (tracking vector). This vector expresses the advection trend, i.e., the movement of the rain cells caused by the wind.

TABLE II
RESULTS

		Rk		
		best	average	worst
including final improvement	no	0.942	0.839	0.739
	yes	0.949	0.865	0.786

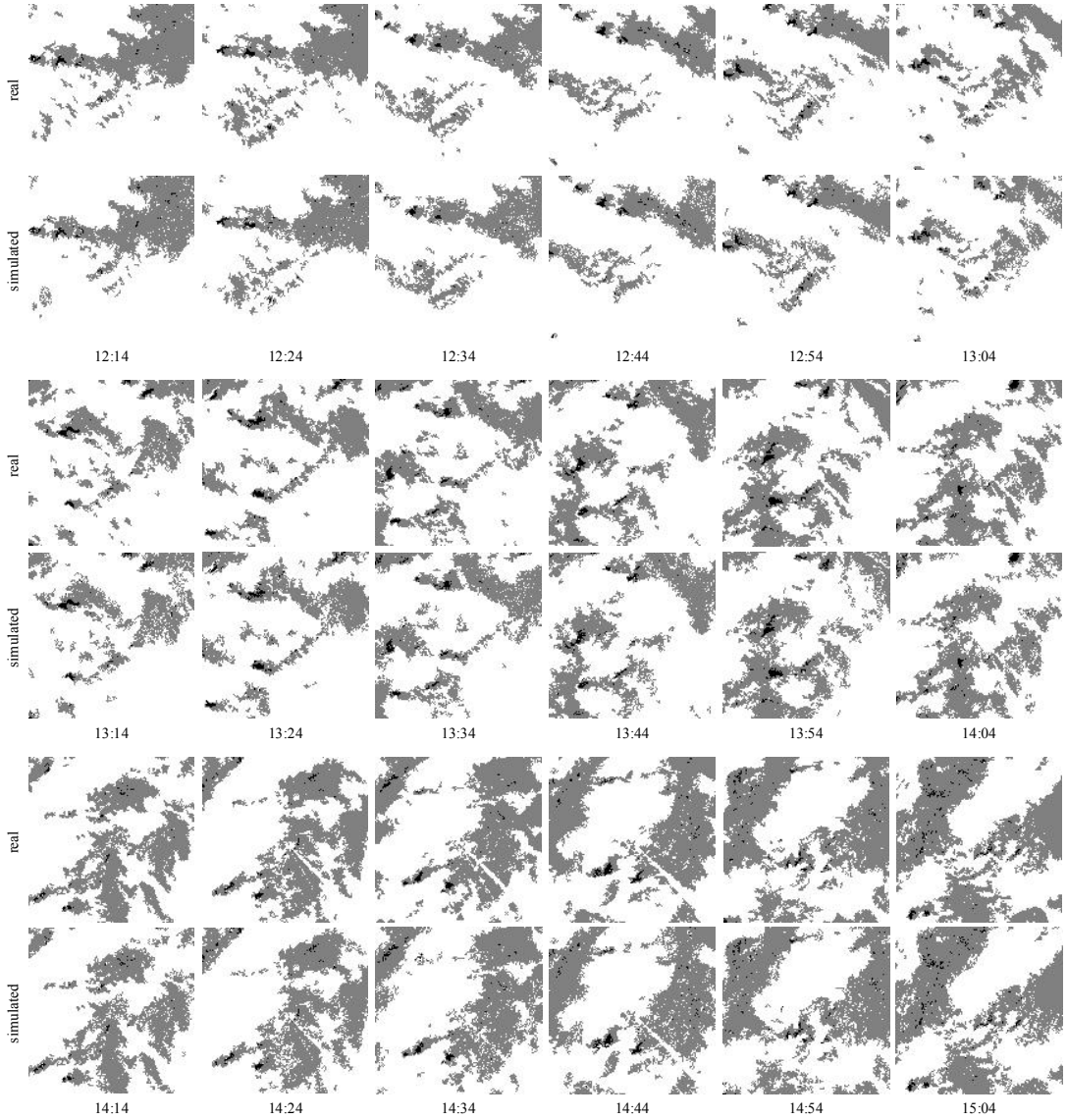

Fig. 3. Real and simulated WRIs occurring on 18 February 2006 between 12:14 and 15:04.

Fig. 3 illustrates both measured and simulated WRIs for one example. Note that the measured WRI at time T has been used to produce the simulated WRI corresponding to time T+1. NR, LR, and HR areas in each WRI are shown in white, grey, and black respectively.

IV. Conclusions

This work focuses on the presentation of an approach for assessing and characterizing rain cell dynamics based exclusively on the analysis of the radar reflectivity images, and without an a priori assumption on the structure of rain cells. This research has been addressed by using cellular automata. Rain cell dynamics are simulated by using probabilistic CA rules and tracking vectors, which indicate a global advection direction and velocity. The proposed method seems to capture with fairly good accuracy the dynamical behavior of rain cells in the studied examples. Moreover, this method offers a global approach to determine the motion for rain cells of WRIs. A straightforward linkage between rain cell dynamics in terms of reflectivity Z (dBz) or its equivalent rain rate R (mm/h) and satellite or terrestrial radiolink attenuation can be performed.

Future work includes expanding the study to other cases, and finding out whether extracting a limited number of general CA rules that capture the rain dynamics in most cases is possible.

Foreseen applications include short time forecasting or nowcasting, e.g., for taking decisions driving fade countermeasures, FCMs, in reconfigurable radio networks, and simulation, e.g., generation of synthetic sequences or ensembles of rain cells for testing radio network performance.

References

[1] COST255: Radiowave propagation modelling for new sitcom services at Ku-band and above, COST255 Final Report, Chapter 2.2 "Rain Attenuation." ESA Publication Division, SP-1252, March 2002.

[2] A. Nuñez, V. Pastoriza, P. Mariño, and F.P. Fontán, "An approach for the modelling of the dynamics in individual raincells cellular automata," Radiowave Propagation Modelling and Measurements for SatCom and SatNav Systems ESA Propagation Workshop, ESA/ESTEC, Noordwijk, The Netherlands, 23-25 November 2005.

[3] J. von Neumann, and A.W. Burks, *Theory of Self-Reproducing Automata*. Urbana, IL: University of Illinois Press, 1966.

[4] S. Ulam, "Some ideas and prospects in Biomathematics," *Annu. Rev. Biophys. Bioeng.,* vol. 1, pp. 277-292, June 1972.

[5] *Cellular automata: Proceeding of an Interdisciplinary Workshop,* D. Farmer, T. Toffoli, and S. Wolfram, Eds. Amsterdam: North Holland Physics Publishing, 1984.

[6] K. Preston, and M. Duff, *Modern Cellular automata*. New York: Plenum, 1984.

[7] *Theory and Applications of Cellular automata,* S. Wolfram, Ed. Singapore: World Scientific, 1986.

[8] F.C. Richards, T.P. Meyer, and N.H. Packard, "Extracting cellular automaton rules directly from experimental data," *Physica D,* vol. 45, pp. 189-202, September 1990.

[9] D. Rosenfeld, E. Amitai, and D.B. Wolf, "Classification of rain regimes by the three-dimensional properties of reflectivity fields," *J. Appl. Meteor.,* vol. 34, pp. 198-211, January 1995.

[10] A. Pawlina, "Essential knowledge of rain structure for radio applications based on available data and models," Radio Africa' 99, 3rd Regional Workshop on Radio Communication in Africa, Gabarone, Botswana, 25-29 October 1999.

[11] T. Mannes, C. Fisher, W. Randeu, K. Koeck, and M. Schoenhuber, "Optimised satellite communications using weather radars," 20th AIAA International Communication Satellite Systems Conference and Exhibit, Montreal, Quebec, May 2002.

[12] C.E. Shannon, and W. Weaver, *The Mathematical Theory of Communication*. Urbana, IL: University of Illinois Press, 1962.

[13] T.M. Cover, and J.A. Thomas, *Elements of Information Theory.* John Wiley & Sons Inc., 1991. Online version: www3.interscience.wiley.com.

[14] J. Gorodkin, "Comparing two K-category assignments by a K-category correlation coefficient," *Comput. Biol. Chem.,* vol. 28 (5-6), pp. 367-374, December 2004.

[15] B.W. Matthews, "Comparison of the predicted and observed secondary structure of T4 Phage Lysozyme," *Biochim. Biophys. Acta,* vol. 405 (2), pp. 442-451, 1975.